

Addressing phase curvature in Fourier ptychography

Tomas Aidukas,¹ Lars Loetgering,^{2,3,4} and Andrew R. Harvey^{1,*}

¹*School of Physics and Astronomy, University of Glasgow, G12 8QQ, UK*

²*Leibniz Institute of Photonic Technology, Albert-Einstein-Straße 9, 07745, Jena, Germany*

³*Helmholtz-Institute Jena, Fröbelstieg 3, 07743 Jena, Germany*

⁴*Institute of Applied Physics and Abbe Center of Photonics, Friedrich Schiller University Jena, Albert-Einstein-Straße 15, 07745 Jena, Germany*

In Fourier ptychography, a theoretical image formation model is used to calculate a wide-field, high-resolution image from the reconstructed sample spectrum. The commonly used far-field assumption connects the source, sample and image planes by Fourier transforms. While computationally simple, this assumption neglects phase curvature due to non-planar illumination from point sources and short propagation distances, which necessitates Fresnel diffraction. We describe a simple, efficient and accurate computational correction of phase curvature during Fourier ptychographic reconstruction. The new method requires only two multiplications: prior and following reconstruction. Quantitative phase reconstruction is now possible even for wide fields-of-view and without the need of image segmentation.

I. INTRODUCTION

Fourier ptychographic microscopy (FPM) is a computational-imaging technique developed for wide-field, high-resolution phase-contrast imaging [1], to overcome the low-pass filtering by the aperture of a microscope. While in traditional microscopy a higher numerical aperture (NA) enables a higher spatial-frequency cut-off (and higher-resolution images), it comes at the cost of reduced field-of-view (FoV). The inverse relationship between FoV and resolution is imposed by the diffraction-limited space-bandwidth-product (SBP) of an imaging system, which defines the total number of independent pixels that can be captured by an imaging system [2]. While low-pass filtering is unavoidable, FPM enables a higher cut-off frequency by capturing multiple and diverse low-resolution bright-field and dark-field images recorded by illuminating from a range of specific angles. These diverse images are coherently combined in the Fourier domain into a wideband image spectrum. The process of synthesising a high-resolution image requires determination of the phases of the angularly-captured images, which are lost during image detection. Phase retrieval thus forms the core of FPM reconstruction algorithms. Image reconstruction can be considered as an optimization problem, minimizing the difference between the experimental measurements and the expected intensity given by the theoretical image formation model. Even for ideal noiseless data, the reconstructed image quality ultimately depends on the accuracy of the forward model being used.

We address two widespread inconsistencies within the FPM image-formation model. Firstly, the conventional FPM model assumes ideal plane-wave illumination, but commonly used point-like LEDs are more appropriately modelled by spherical wavefronts. A spherical surface

can be approximated as planar over a sufficiently narrow FoV area, which is why the commonly used “segment-reconstruct-stitch” [1, 3] approach is able to partially mitigate this problem. However, we will show that significant phase curvature can be expected even for very small FoV segments. Secondly, an additional phase curvature commonly appears in the reconstructed (complex) images due to Fresnel diffraction during image formation. We introduce a theoretical model to incorporate curvature correction into FPM, which has not been correctly described in the existing FPM literature. Our proposed computational correction requires only two multiplications prior and after the reconstruction, resulting in a minor increase in computational complexity while drastically improving the quality of reconstructed images.

II. PHASE CURVATURE MODEL

The standard image-formation model in FPM assumes that the sample $o(\mathbf{r})$ is illuminated with plane-waves to produce the diffracted sample spectrum $O(\mathbf{k})$. With plane-wave illumination, the sample spectrum is translated in the pupil plane by \mathbf{k}_i . The translated spectrum is low-pass filtered by the pupil $P(\mathbf{k})$ and propagated to the image plane. The intensity for illumination by the i^{th} LED is [1]:

$$I_i(\mathbf{r}) = |\mathcal{F}\{P(\mathbf{k})O(\mathbf{k} - \mathbf{k}_i)\}|^2. \quad (1)$$

By synthesizing multiple experimental images in the Fourier domain, a broadband spectrum $O(\mathbf{k})$ can be calculated and a high-SBP sample image $o(\mathbf{r})$ can be reconstructed. Typically, the far-field diffraction assumption is used to describe the transformation between the reconstructed sample image and its spectrum [1, 4]:

$$O(\mathbf{k}) = \mathcal{F}\{o(\mathbf{r})\}. \quad (2)$$

* andy.harvey@glasgow.ac.uk

However, due to modest propagation distances and wide FoV areas (common to FPM), this assumption is an oversimplification.

The classical image formation model derived using Fresnel diffraction [5] contains a phase curvature term $Q(\mathbf{r})$ (to be specified below)

$$O(\mathbf{k}) = \mathcal{F}\{o(\mathbf{r})Q(\mathbf{r})\}. \quad (3)$$

Moreover, Eqn. 1 assumes plane-wave illumination, whereas in FPM a LED array is typically used, resulting in a curved, rather than a planar wavefront incident on the specimen. While it was shown that telecentric lenses can be used to mitigate illumination curvature [6], we can instead computationally incorporate it in a modified definition for $Q(\mathbf{r})$:

$$Q(\mathbf{r}) = \exp\left(ik\left(\frac{1}{2u} + \frac{1}{2z}\right)(x^2 + y^2)\right). \quad (4)$$

Within $Q(\mathbf{r})$ there are two contributions: illumination phase curvature, Q_{ill} (proportional to $1/z$), and phase curvature due to Fresnel diffraction during image formation, Q_p (proportional to $1/u$), as illustrated in Fig. 1(a). Here, z is the distance from the LED to the sample plane and u is the distance from the sample to the pupil plane, where we assume a single-lens FPM system (where the lens and pupil planes coincide). Figures Fig. 1(b) and (c) illustrate the effect of phase curvature over varying FOVs in a typical microscope (the figures were generated based on our experimental setup described in the next section). Since phase curvature is visible even for very small FoV segments, computational correction is important even when using the segmentation-based reconstruction. It should be emphasized that the main strength of FPM is the computational ability to improve the resolution of low-NA lenses, which are used for wide-FoV imaging. In addition, the distance from the LED array to the sample (z) determines how frequency bands from adjacent illumination sources overlap in Fourier domain. Since FPM reconstruction requires the overlap to be at least 60% [7], the propagation distance z and the imaging FoV cannot be arbitrarily modified to remove phase curvature effects.

From Eqn. 1 it is seen that recording data in the image plane is not sensitive to the phase curvature $Q(\mathbf{r})$. In particular, the absolute value squared operation renders a direct observation of the quadratic phase impossible. It may thus seem that we could simply ignore it, without affecting the underlying FPM model, quantified by a suitable cost function measuring the deviation between the observation and estimated parameters [8–10]. One example of such a cost function for a given illumination i can be written as the L2-norm between the measured and expected amplitude:

$$\mathcal{L}_i = \left\| \sqrt{I_i(\mathbf{r})} - |\mathcal{F}\{P(\mathbf{k})O(\mathbf{k} - \mathbf{k}_i)\}| \right\|^2. \quad (5)$$

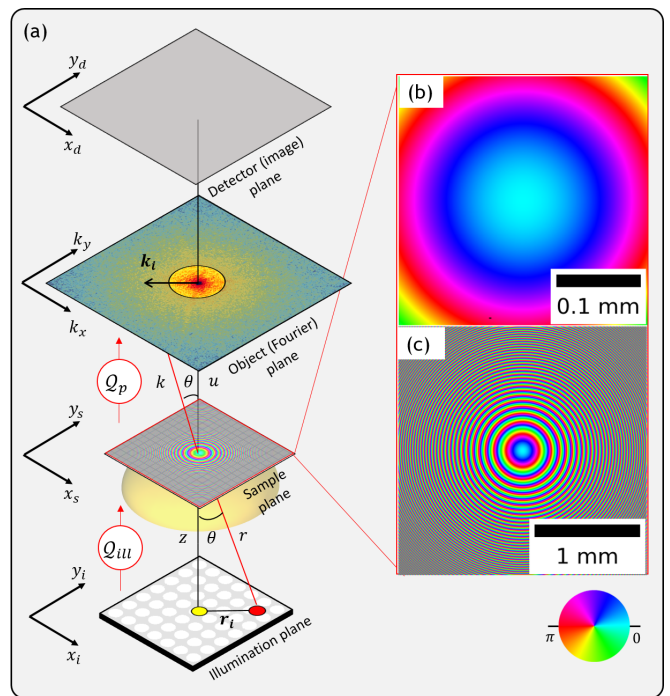


FIG. 1. (a) The origin of the phase curvature is due to spherical-wave illumination and sample-to-lens wave propagation. Phase curvature severity will ultimately depend on the propagation distance and FoV area. When using segmentation-based reconstruction, the narrow-FoV of each segment will contain minimal phase curvature, as shown in (b). However, the same cannot be told about wide-FoVs where phase curvature becomes extremely warped, as shown in (c). The FoV shown here, is only half of the total sensor area, hence the actual phase curvature in our experiments is even greater.

However, the quadratic phase within $Q(\mathbf{r})$ does affect the reconstruction of the spectrum $O(\mathbf{k})$, which FPM seeks to stitch together in a self-consistent way by minimizing \mathcal{L}_i . We will demonstrate below that neglecting $Q(\mathbf{r})$ leads to a poor initialization of the underlying forward model, which can prevent convergence to a feasible solution.

III. PHASE CURVATURE CORRECTION

We obtain an initial estimate for our FPM reconstruction by means of the following steps: First, the mean over all captured images is computed. Second, the aforementioned mean image is upsampled to the pixel size of the high-NA synthetic Fourier space resulting from all illumination directions, resulting in $o_{\text{init}}(\mathbf{r})$. Third, we embed phase curvature into the FPM forward model as described by Eqn. 3 and Eqn. 4, leading to:

$$O_{\text{init}}(\mathbf{k}) = \mathcal{F}\{o_{\text{init}}(\mathbf{r})Q(\mathbf{r})\}, \quad (6)$$

which serves as the initial estimate for the FPM reconstruction. The reconstructed $O_R(\mathbf{k})$ is back-propagated

into the sample plane, where the quadratic phase is conjugated out to obtain the reconstructed sample $o_R(\mathbf{r})$:

$$o_R(\mathbf{r}) = \mathcal{F}^{-1} \{O_R(\mathbf{k})\} Q^*(\mathbf{r}). \quad (7)$$

As will be shown in the next section, this initialization procedure is a crucial ingredient for stable reconstruction of both narrow- and wide-field images in FPM.

IV. VALIDATION OF THE MODEL

For both the simulations and experimental data reconstructions we used the microscope previously reported in [11]. The data was captured with illumination directions from 21×21 LEDs (“Adafruit LED array”) with a wavelength of $\lambda = 630nm$ and $5mm$ pitch of the LEDs. The microscope used a $8mm$ diameter and $36mm$ focal length achromatic lenses from “Edmund optics”. For image recording, we used “DMM 37ux264-ML” 2448×2048 5-megapixel monochrome sensor boards with a $3.45\mu m$ pixel size from “The Imaging Source”. The sample-to-lens distance, and LED-to-sample distance were $u = 60mm$ and $z = 120mm$ respectively, which are relatively large for a conventional microscope, indicating that more severe curvatures can be expected in typical FPM systems. Given these experimental parameters, the numerical aperture was 0.065, resulting in the raw image resolution of $9.6\mu m$. By synthesizing 21×21 angularly illuminated images through FPM reconstruction, the synthetic numerical aperture was 0.365 equivalent to $1.45\mu m$ resolution, which we demonstrated in [11, 12].

To validate the correction strategy, simulations were performed by the method outlined in Sec. VIII C. This simulation method enables the inclusion of phase curvature due to Fresnel diffraction to the lens plane and point source illumination assumption (spherical-waves). We simulated a Siemens star target with a FoV size of $0.3mm$ (128×128 pixels, see Fig. 2(a)) and $2mm$ (1024×1024 pixels, Fig. 2(b)). The data consisted of images recorded at 49 illumination angles. Even for the small FoV size of $0.3mm$ (128×128 pixels), conventional FPM reconstruction produces phase maps which have a root-mean-squared (RMS) error of 0.41 compared to the simulated phase, whereas with our proposed correction method the error is reduced to 0.04. Increasing FoV size up to $\sim 2mm$ (1024×1024 pixels) results in severely distorted phase curvature, where the reconstructed image phase has an RMS errors of 0.84 without correction and 0.07 with correction.

We illustrate the need for phase curvature correction (Fig. 3(a)) for both segmentation-free and segmentation-based reconstructions using a lung carcinoma sample shown in Fig. 3(b). In the segmentation-based reconstruction shown in Fig. 3(c1-c2), the 1024×1024 pixels for the full FoV were divided into smaller 128×128 pixel

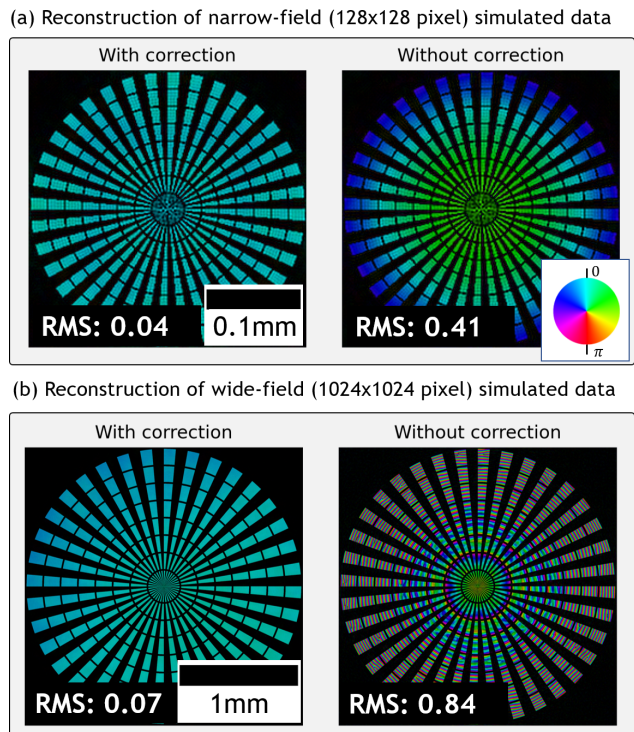


FIG. 2. FPM data was simulated for FOV sizes of (a) 128×128 and (b) 1024×1024 pixels. While phase curvature varies with FOV size, it is significant even for the small FOV. For wide-field reconstruction, phase curvature is large enough that severe phase wrapping occurs. In both cases, the computational correction method was able to reconstruct images free of phase curvature compared to basic FPM reconstructions without the proposed correction method. The root-mean-square (RMS) values were given to quantify reconstructed image deviations from the ideal phase.

($0.3mm \times 0.3mm$) segments to reduce spatially varying aberrations and phase-curvature. Once reconstructed, all segments were tiled together into a single wide-field, high-resolution image. Without correction (Fig. 3(c1)), each reconstructed tile contains minor phase curvature, resulting in a distorted phase map of the sample. Once corrected (Fig. 3(c2)), the tiles can be seamlessly stitched together without any visible phase discontinuities.

In the segmentation-free reconstruction Fig. 3(d1-d2), the full-FoV was reconstructed in a single step. Due to the missing phase curvature initialization, Fig. 3(d1) displays significant phase inconsistencies. While it would be convenient to simply use conventional FPM methods and multiply out the phase curvature post-reconstruction, the inconsistencies in panel (d1) would remain, which renders this processing route infeasible. In Fig. 3(d2) we followed our proposed initialization approach on the large field of view. This reconstruction is free of the phase artefacts observed in panel (d1). Moreover, the reconstruction in panel (d2) is consistent with the segmentation-based reconstruction in (c2).

Lastly, we have also validated the proposed method on

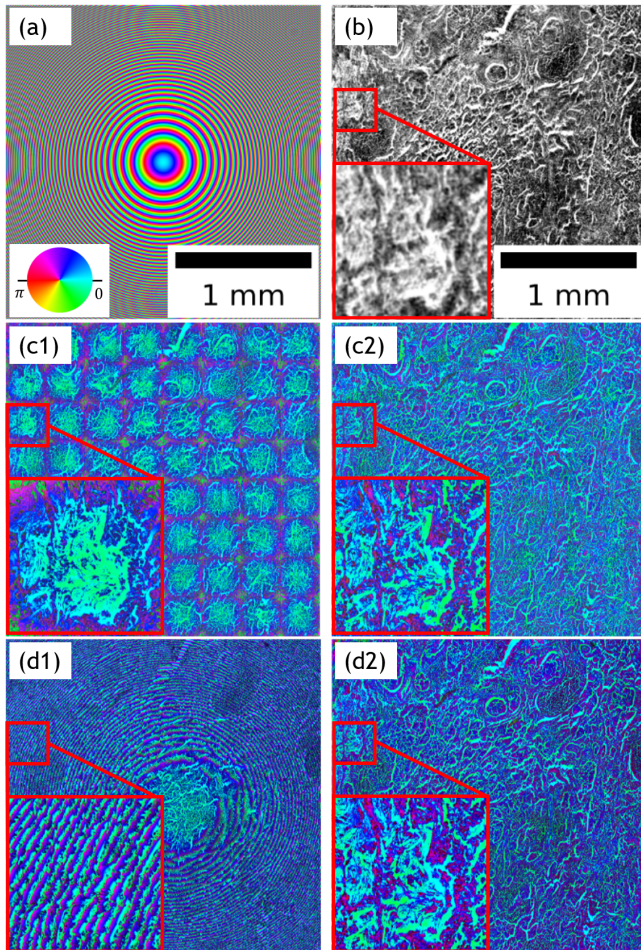


FIG. 3. Simulated phase curvature in (a) is expected in the reconstructions of a Lung Carcinoma sample 1024×1024 pixel FoV shown in (b). When FoV is divided into 128×128 pixel tiles, the phase curvature is minimized, but not eliminated in the segmentation-based reconstruction shown in (c1), necessitating the need for correction in (c2). In segmentation-free reconstruction, phase curvature is severely wrapped due to wide-FoV of 1024×1024 pixels shown in (d1) and the corresponding correction in (d2). In both narrow and wide FoV reconstructions, our proposed method is able to eliminate phase curvature.

a different experimental setup, whose optical design parameters and data available are publicly available in [13]. The low-cost microscope was equipped with a Raspberry Pi V2 NOIR camera module (8-megapixels, $1.12 \mu\text{m}$ pixel size) which also contains a 3-mm focal-length camera lens. The frequency overlap of 70% (required for FPM reconstruction) was obtained by placing the Unicorn HAT HD 16×16 LED array (3.3mm pitch) 60mm below the sample stage. The low-resolution microscope has 0.15 NA and a 7mm working distance, whereas the synthetic NA achieved after FPM reconstruction was 0.55 (see [13]).

As expected, the reconstructed images shown in

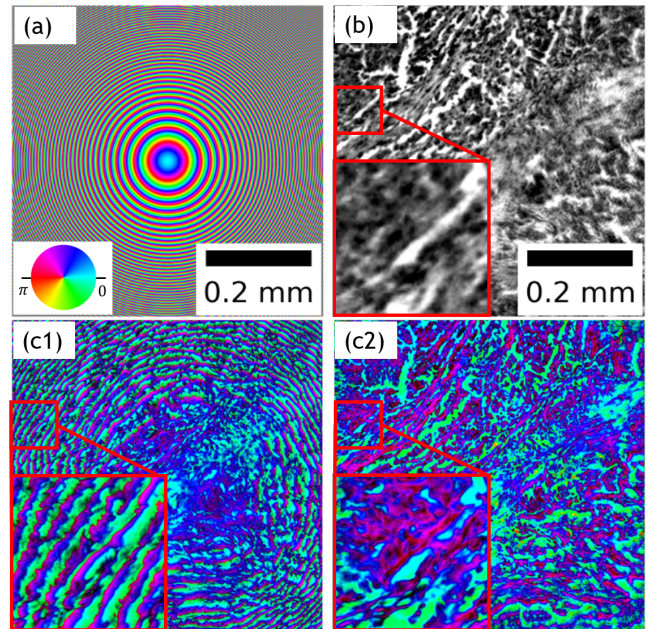


FIG. 4. Results from a low-cost FPM microscope published in [13], showing the expected phase curvature (a) within the reconstruction of a Lung Carcinoma sample (b). Segmentation-free reconstruction exhibits the expected phase curvature in (c1) while the proposed correction in (c2) is able to eliminate it.

Fig. 4(c1-c2) exhibit phase curvature of similar severity to the previously shown results in Fig. 4(d1-d2). Moreover, being a low-cost microscope, optical aberrations and low signal-to-noise ratio inhibit reconstruction convergence. Combined with the incorrect image formation model the reconstruction fails completely as shown in Fig. 4(c1)), whereas the previous less aberrated microscope only the phase maps are affected in Fig. 4(d1) (the central FoV area is reconstructed well). These observations demonstrate that phase curvature not only cosmetically affect the recovered phase maps, but also FPM reconstruction convergence properties.

V. CONCLUSION

We have shown that our proposed method achieves improved phase estimation in FPM, by including illumination phase curvature and Fresnel diffraction effects into FPM forward model. Surprisingly, this rather simple but important modelling step has not been reported to date. The initialization method proposed here is simple and computationally efficient, requiring only two multiplications prior to and following reconstruction (similar to quadratic phase correction strategies used in digital holography [14, 15]). Not only does the correction remove the phase curvature artefacts, but also improves algorithmic convergence, since reconstruction of the phase curvature itself is no longer required. The reduced computa-

tional burden is especially important when using highly aberrated optics [3, 13], where the need to recover both the aberrations and phase-curvature is likely to result in reconstruction failure. Moreover, if image formation can be assumed spatially-invariant, segmentation-free reconstruction can be performed without visible phase curvature, which is crucial for quantitative phase imaging. In summary, the proposed method improves algorithmic convergence and bypasses time-consuming stitching as well as phase synchronization of adjacent sample regions

in segmentation-based FPM.

VI. DISCLOSURES

The authors declare no conflicts of interest.

VII. DATA AVAILABILITY

A current version of the data analysis software is available upon request from the corresponding authors.

-
- [1] G. Zheng, R. Horstmeyer, and C. Yang, Wide-field, high-resolution fourier ptychographic microscopy, *Nature photonics* **7**, 739 (2013).
- [2] P. C. Konda, L. Loetgering, K. C. Zhou, S. Xu, A. R. Harvey, and R. Horstmeyer, Fourier ptychography: current applications and future promises, *Opt. Express* **28**, 9603 (2020).
- [3] G. Zheng, X. Ou, R. Horstmeyer, and C. Yang, Characterization of spatially varying aberrations for wide field-of-view microscopy, *Optics express* **21**, 15131 (2013).
- [4] R. Horstmeyer, *Computational microscopy: Turning megapixels into gigapixels* (2016).
- [5] J. W. Goodman, *Introduction to Fourier optics* (Roberts and Company Publishers, 2005).
- [6] Y. Zhu, M. Sun, X. Chen, H. Li, Q. Mu, D. Li, and L. Xuan, Single full-fov reconstruction fourier ptychographic microscopy, *Biomed. Opt. Express* **11**, 7175 (2020).
- [7] J. Sun, Q. Chen, Y. Zhang, and C. Zuo, Sampling criteria for Fourier ptychographic microscopy in object space and frequency space, *Optics Express* **24**, 15765 (2016).
- [8] M. Odstrčil, A. Menzel, and M. Guizar-Sicairos, Iterative least-squares solver for generalized maximum-likelihood ptychography, *Opt. Express* **26**, 3108 (2018).
- [9] L.-H. Yeh, J. Dong, J. Zhong, L. Tian, M. Chen, G. Tang, M. Soltanolkotabi, and L. Waller, Experimental robustness of fourier ptychography phase retrieval algorithms, *Optics express* **23**, 33214 (2015).
- [10] P. Thibault and M. Guizar-Sicairos, Maximum-likelihood refinement for coherent diffractive imaging, *New Journal of Physics* **14**, 063004 (2012).
- [11] T. Aidukas, P. C. Konda, and A. R. Harvey, High-speed fourier ptychography utilizing multiple-cameras and led multiplexing (Optical Society of America, Washington, DC, 2021) p. CTu6A.3.
- [12] T. Aidukas, *Next generation Fourier ptychographic microscopy: computational and experimental techniques*, Ph.D. thesis, University of Glasgow, School of Physics and Astronomy (2021).
- [13] T. Aidukas, R. Eckert, A. R. Harvey, L. Waller, and P. C. Konda, Low-cost, sub-micron resolution, wide-field computational microscopy using opensource hardware, *Scientific reports* **9**, 1 (2019).
- [14] E. Cuche, P. Marquet, and C. Depeursinge, Simultaneous amplitude-contrast and quantitative phase-contrast microscopy by numerical reconstruction of fresnel off-axis holograms, *Appl. Opt.* **38**, 6994 (1999).
- [15] S. T. Thurman and J. R. Fienup, Phase-error correction in digital holography, *J. Opt. Soc. Am. A* **25**, 983 (2008).
- [16] T. Salditt and A.-L. Robisch, Coherent x-ray imaging, in *Nanoscale Photonic Imaging*, edited by T. Salditt, A. Egner, and D. R. Luke (Springer International Publishing, Cham, 2020) pp. 35–70.

VIII. SUPPLEMENTARY MATERIAL

A. Plane-wave illumination

We assume that the sample $o(\mathbf{r}_s)$ is illuminated by plane waves originating from $\mathbf{r}_i = (x_i, y_i)$ with respect to the sample $\mathbf{r}_s = (x_s, y_s)$ based on the geometry from Fig. 1(a). We assume that the sample $o(\mathbf{r}_s)$ is illuminated by plane waves originating from $\mathbf{r}_i = (x_i, y_i)$ with respect to the sample $\mathbf{r}_s = (x_s, y_s)$ based on the geometry from Fig. 1(a). To simplify the analysis of wave interaction with matter, it will be assumed that the sample is thin [16]. Also, neglecting diffraction effects within the sample, light scattering by the sample can be expressed by the projection approximation [16]:

$$o'(\mathbf{r}_s) = p(\mathbf{r}_s)o(\mathbf{r}_s), \quad (8)$$

where $o'(\mathbf{r})$ describes a sample $o(\mathbf{r})$ illuminated by $p(\mathbf{r})$. The simplest illumination model is a plane-wave defined as a ‘‘phase ramp’’:

$$p(\mathbf{r}_s) = \exp(i\mathbf{k}_i\mathbf{r}_s) = \exp(i(k_{x,i}x_s + k_{y,i}y_s)). \quad (9)$$

The unique feature of a plane-wave is a transverse phase shift for a given \mathbf{k} -vector \mathbf{k}_i and the property $|\mathbf{k}| = k = 2\pi/\lambda$. A phase ramp corresponds to translation in spatial frequency following Fourier transformation. This concept is heavily exploited by FPM, in which \mathbf{k} -vectors are manipulated by changing the angle of illumination to shift the diffracted spectrum. To show this effect, we start by propagating a diffracted wavefront $o'(\mathbf{r})$ to the lens plane using a Fresnel diffraction integral [5]:

$$\begin{aligned} \psi(\mathbf{r}_l) &= \frac{\exp(iku)}{i\lambda u} \exp\left(\frac{ik}{2u}(x_l^2 + y_l^2)\right) \iint o'(x_s, y_s) \\ &\quad \exp\left(\frac{ik}{2u}(x_s^2 + y_s^2)\right) \exp(-i(k_{x,i}x_s + k_{y,i}y_s)) dx_s dy_s. \end{aligned} \quad (10)$$

The phase factors preceding the integral will be neglected for brevity. Inserting an expression for $o'(x_s, y_s)$ into Eqn. 10:

$$\begin{aligned} \psi(\mathbf{r}_l) &= \iint o(x_s, y_s) \exp\left(\frac{ik}{2u}(x_s^2 + y_s^2)\right) \\ &\quad \exp(-i((k_x - k_{x,i})x_s + (k_y - k_{y,i})y_s)) dx_s dy_s \\ &= \mathcal{F} \left\{ o(x_s, y_s) \exp\left(\frac{ik}{2u}(x_s^2 + y_s^2)\right) \right\}_{(\mathbf{k}-\mathbf{k}_i)} \\ &= O(\mathbf{k} - \mathbf{k}_i). \end{aligned} \quad (11)$$

The exit-wave $\psi(\mathbf{r}_l)$ represents scattered light (in the lens plane) from the sample $o(\mathbf{r})$. This expression is the same as the one derived for conventional image formation [5],

with additional frequency spectrum translation by \mathbf{k}_i :

$$O(\mathbf{k} - \mathbf{k}_i) = \mathcal{F} \left\{ o(\mathbf{r}_s) \exp\left(\frac{ik}{2u}(x_s^2 + y_s^2)\right) \right\} \quad (12)$$

This expression shows that the translated spectrum is equivalent to the Fourier transform of the sample multiplied with a quadratic phase term due to Fresnel diffraction. If the propagation distance u is insufficient with respect to the sample area (x_s, y_s) , then the quadratic phase appears as an artefact in reconstructed images.

B. Spherical-wave illumination

While plane waves are idealized mathematical objects, the plane-wave assumption holds for sufficiently small FOVs in real-world applications. If the approximation is broken, the frequency translation for a given illumination angle can no longer be considered to be linear. The use of non-planar illumination requires a more general description, which can be provided by assuming illumination from a point-source. In this case, each LED can be assumed as a source of spherical waves [5], defined as

$$p(\mathbf{r}_s) = \exp(ikr). \quad (13)$$

Distance r defines the propagation distance between source $\mathbf{r}_i = (x_i, y_i)$ and destination $\mathbf{r}_s = (x_s, y_s)$ planes given by the geometry in Fig. 1(a):

$$\begin{aligned} r = |\mathbf{r}_s - \mathbf{r}_i| &= \sqrt{(x_s - x_i)^2 + (y_s - y_i)^2 + z^2} \\ &= z \sqrt{1 + \frac{(x_s - x_i)^2 + (y_s - y_i)^2}{z^2}}, \end{aligned} \quad (14)$$

where z defines the distance from the LED array to the sample plane. To simplify the expression, we can decompose r into multiple terms using a Taylor expansion and truncating higher order terms:

$$\begin{aligned} r &\approx z + \frac{(x_s - x_i)^2 + (y_s - y_i)^2}{2z} \\ &= z + \frac{x_s^2 + y_s^2}{2z} + \frac{x_s x_i + y_s y_i}{z} + \frac{x_i^2 + y_i^2}{2z}. \end{aligned} \quad (15)$$

Using this approximation for r , the spherical-wave expression in Eqn. 13 can be written as:

$$\begin{aligned} p(\mathbf{r}_s) &= \exp(ikz) \exp\left(ik \frac{x_s^2 + y_s^2}{2z}\right) \\ &\quad \exp\left(-ik \frac{x_s x_i + y_s y_i}{z}\right) \exp\left(ik \frac{x_i^2 + y_i^2}{2z}\right). \end{aligned} \quad (16)$$

Terms $\exp(ikz)$ and $\exp\left(ik \frac{x_i^2 + y_i^2}{2z}\right)$ are constant for each point in the sample plane and can be neglected, reducing

Eqn. 16 to:

$$\begin{aligned} p(\mathbf{r}_s) &= \exp\left(\frac{ik}{2z}(x_s^2 + y_s^2)\right) \exp\left(-ik\frac{x_s x_i + y_s y_i}{z}\right) \\ &= \exp\left(\frac{ik}{2z}(x_s^2 + y_s^2)\right) \exp(-i(k_{x,i}x_s + k_{y,i}y_s)), \end{aligned} \quad (17)$$

where Fourier domain wave vectors were introduced by the following substitution:

$$k_{x,i} = kx_i/z, \quad k_{y,i} = ky_i/z. \quad (18)$$

Comparing the plane-wave expression from Eqn. 9 to spherical waves in Eqn. 17 the only difference is an additional quadratic phase factor:

$$\exp\left(\frac{ik}{2z}(x_s^2 + y_s^2)\right). \quad (19)$$

Following derivations used for plane-wave illumination, the additional quadratic phase factor will be absorbed by the diffracted spectrum in Eqn. 12 leading to:

$$\begin{aligned} O(\mathbf{k} - \mathbf{k}_i) &= \mathcal{F} \left\{ o(\mathbf{r}_s) \exp\left(ik\left(\frac{1}{2u} + \frac{1}{2z}\right)(x_s^2 + y_s^2)\right) \right\} \\ &= \mathcal{F} \{ o(\mathbf{r}_s) Q(\mathbf{r}_s) \} \end{aligned} \quad (20)$$

Based on Eqn. 20 and Eqn. 12, both plane-waves and spherical-waves translate the sample spectrum by \mathbf{k}_i . In addition, phase curvature from Eqn. 20 can be written as:

$$Q(\mathbf{r}_s) = \exp\left(ik\left(\frac{1}{2u} + \frac{1}{2z}\right)(x_s^2 + y_s^2)\right) \quad (21)$$

C. Image simulation

Angular sample illumination in FPM will result in spectrum translation within the Fourier domain. This can be performed by simulating either plane-wave (Eqn. 9) or spherical-wave (Eqn. 13) illumination:

$$\begin{aligned} p(\mathbf{r}) &= \exp(i\mathbf{k}_i\mathbf{r}) && \text{Plane-wave} \\ p(\mathbf{r}) &= \exp(ikr) && \text{Spherical-wave} \end{aligned}$$

In this manuscript, we assumed that the sample is illuminated by LEDs modelled as point-sources of spherical illumination wavefronts. The scattered wavefronts were then propagated from the sample plane to the detector

plane using typical Fresnel propagators [5]:

$$\begin{aligned} \mathcal{P}_z(f(x', y')) &= \frac{\exp(ikz)}{i\lambda z} \exp\left(\frac{ik}{2z}(x^2 + y^2)\right) \\ &\quad \mathcal{F} \left\{ f(x', y') \exp\left(\frac{ik}{2z}(x'^2 + y'^2)\right) \right\}. \end{aligned} \quad (22)$$

This expression can be used to propagate an optical field $f(x', y')$ by a distance z from the plane (x', y') to (x, y) . In the lens plane, the lens will interact with incident wavefronts not only by filtering the frequencies (due to finite pupil aperture), but also by introducing the following quadratic phase factor [5]:

$$Q_{\text{lens}} = \exp\left(\frac{-ik}{2f}(x^2 + y^2)\right). \quad (23)$$

In conventional imaging the lens is carefully chosen such that the quadratic phase terms introduced by the propagator \mathcal{P}_z can be cancelled out by Q_{lens} . The propagation steps to produce an intensity image for a given illumination angle are outlined in Alg. 1 to mimic the conventional image formation model [5]:

- Create a scattered wavefront as a result of sample illumination (Eqn. 8), which will also impart a phase shift resulting in Fourier domain spectrum translation (due to angular illumination) as described in Eqn. 20.
- Propagate the wavefront from the sample to the lens plane by using Fresnel diffraction propagator from Eqn. 22.
- Perform frequency filtering by the pupil $P(\mathbf{k})$ and apply a phase transformation due to interaction with the lens $Q_{(\text{lens})}$.
- Propagate to the detector plane using Eqn. 22, transforming the diffracted fields back into the spatial domain.
- Perform image detection by $|\cdot|^2$.

Algorithm 1 Simulation pseudocode.

```

Initialize spatial illumination coordinates, sample and pupil:  $\mathbf{r}_i, o(\mathbf{r}), P(\mathbf{k})$ 
for  $i, \forall i \in [1, \dots, I]$  do
  Create illuminating wavefront:  $p(\mathbf{r})$ 
  Compute a scattered wavefront:  $o'(\mathbf{r}) = o(\mathbf{r})p(\mathbf{r})$ 
  Propagate to the lens plane:  $O(\mathbf{k}) = \mathcal{P}_z(o'(\mathbf{r}))$ 
  Low-pass filter:  $O'(\mathbf{k}) = O(\mathbf{k})P(\mathbf{k})Q_{\text{lens}}$ 
  Propagate to the detector plane:  $o''(\mathbf{r}) = \mathcal{P}_z(O'(\mathbf{k}))$ 
  Compute and save the image:  $I_i(\mathbf{r}) = |o''(\mathbf{r})|^2$ 
end for

```
